Supplementary Material for: Investigation of blood rheology under steady and unidirectional large amplitude oscillatory shear

Jeffrey S. Horner[a)], Matthew J. Armstrong[b)], Norman J. Wagner[a)], and Antony N. Beris[a)*]

[a)]Center for Molecular and Engineering Thermodynamics and Department of Chemical and Biomolecular Engineering, University of Delaware, Newark, DE 19716
[b)]Department of Chemistry and Life Science, United States Military Academy, West Point, NY 10996
[*]Author to whom correspondence should be addressed; electronic mail: beris@udel.edu

S-I. AAB MODEL FORMULATION

The AAB model used throughout this work as a comparison is a specific example of the MDTM for human blood rheology [5,25,30]. For steady state, the model assumes a Casson behavior at low to moderate shear rates:

$$\sigma^{\frac{1}{2}} = \sigma_y^{\frac{1}{2}} + (\mu\dot{\gamma})^{\frac{1}{2}} . \tag{S1}$$

The yield stress, σ_y (in dyne/cm^2), and the model viscosity, μ, may be determined from the fibrinogen concentration, c_f (in g/dL), and the hematocrit, Hct, of the blood sample according to the following parametric equations:

$$\sigma_y = \begin{cases} (Hct - Hct_c)^2 \times \left(0.5084 c_f + 0.4517\right)^2, & Hct > Hct_c \\ 0, & Hct \le Hct_c \end{cases} \tag{S2}$$

$$Hct_c = \begin{cases} 0.3126 c_f^2 - 0.468 c_f + 0.1764, & cf < 0.75 \\ 0.0012, & c_f \ge 0.75 \end{cases} \tag{S3}$$

$$\mu = \mu_p (1 + 2.0703 Hct + 3.7222 Hct^2) \times \exp\left(-7.0276\left(1 - \frac{T_0}{T}\right)\right), \tag{S4}$$

where μ_p is the plasma viscosity, T_0 is the reference temperature at which the plasma viscosity is measured (in K), and T is the temperature of the blood sample (in K).

For the transient behavior of the model, the stress is specified as a summation of an elastic stress and a viscous stress without a direct dependence on the structural parameter:

$$\sigma = G\gamma_e + \mu\dot{\gamma}_p . \tag{S5}$$

The structure parameter affects the stress indirectly through the elastic modulus which evolves through a relaxation rate equation:

$$\frac{dG}{dt} = \frac{\sigma_y}{\mu} k_G \lambda \left(\frac{\sigma_y}{\gamma_0}\lambda - G\right), \tag{S6}$$

where k_G is a nondimensional rate parameter for the relaxation of the elastic modulus. This formulation differs from the new model proposition by featuring a dependence of the rate of relaxation on the structure

parameter, λ, and an elastic modulus equilibrium value that is linearly proportional to the structure parameter as opposed to inversely proportional.

The structure parameter evolves through a similar structural kinetic rate equation:

$$\frac{d\lambda}{dt} = \frac{\sigma_y}{\mu} k_\lambda \left((1-\lambda) - \lambda \sqrt{\frac{4\mu\dot{\gamma}_p}{\sigma_y}} \right), \tag{S7}$$

where k_λ is a nondimensional rate parameter for the evolution of the structure parameter. Unlike the new model, this formulation lacks a shear induced aggregation term. Additionally, due to the assumption of Casson behavior under steady shear, the time constants are specified and characteristic exponents are specified differently.

Identical to the new model, the total strain and rate of strain in the AAB model are decomposed into an elastic and plastic component as outlined in Eq. (16) of the main text. The plastic rate of strain evolves according to Eq. (19) in the main text. However, the elastic rate of strain differs in that the AAB model does not include a term to account for the breakup of structure:

$$\dot{\gamma}_e = \dot{\gamma}_p - \frac{\gamma_e}{\gamma_{max}} \left| \dot{\gamma}_p \right| . \tag{S8}$$

Additionally, the maximum elastic strain is defined according to:

$$\gamma_{max} = \min \left(\frac{\gamma_0}{\lambda^2}, \gamma_\infty \right), \tag{S9}$$

where γ_∞ is a parameter representing the infinite shear limiting value for the maximum elastic strain. Unlike the new model, the maximum elastic strain in the AAB model is inversely proportional to the structural parameter and features a finite limiting value for the limit of high shear rates. This finite limiting value gives rise to a transition from Casson behavior to Newtonian behavior at high shear rates as exhibited by the steady state solution to the model:

$$\sqrt{\sigma_{SS}} = \begin{cases} \sqrt{\sigma_y} + \sqrt{\mu\dot{\gamma}}, & \sqrt{\frac{4\mu\dot{\gamma}}{\sigma_y}} < \sqrt{\frac{\gamma_\infty}{\gamma_0}} - 1 \\ \sqrt{\frac{\sigma_y}{\sqrt{\frac{4\mu\dot{\gamma}}{\sigma_y}}+1} \frac{\gamma_\infty}{\gamma_0} + \mu\dot{\gamma}}, & \sqrt{\frac{4\mu\dot{\gamma}}{\sigma_y}} \geq \sqrt{\frac{\gamma_\infty}{\gamma_0}} - 1 \end{cases} . \tag{S10}$$

In total, the AAB features six model parameters (μ, σ_y, k_λ, k_G, γ_0, and γ_∞), two of which (μ and σ_y) may be predicted from the physiological data. Overall, the AAB model is advantageous over the newly proposed model due to its relation to the physiology and fewer parameters. However, these advantages are outweighed by the poor fit to experimental data over a wide range of flow conditions. The model is unable to properly capture the UD-LAOS data largely due to the assumption of Casson behavior and the disappearance of elastic effects at high shear rates.

S-II. DERIVATION OF THE VISCOELASTIC RED BLOOD CELL MODEL

We begin the derivation of the red blood cell viscoelastic model by starting with the extended White-Metzner model, previously shown in Eq. (3) in the main text:

$$\boldsymbol{\sigma_C} + \left(\frac{\eta_C(c_I)}{G_C}\right)\boldsymbol{\sigma_C}_{(1)} = \eta_C(c_I)\boldsymbol{\gamma}_{(1)} \,. \tag{S11}$$

For a detailed derivation of how the extended White-Metzner model can be obtained through a first principles conformation tensor approach, the reader is referred to Souvaliotis and Beris [46]. For one dimensional shear flow, there are only two nonzero, unique elements of the stress tensor:

$$\boldsymbol{\sigma_C} = \begin{pmatrix} \sigma_{11,C} & \sigma_{12,C} & 0 \\ \sigma_{12,C} & 0 & 0 \\ 0 & 0 & 0 \end{pmatrix}. \tag{S12}$$

Using Eq. (4) in the main text, we can also define the conformation tensor as:

$$\boldsymbol{c} = \frac{1}{G_C}\begin{pmatrix} \sigma_{11,C} + G_C & \sigma_{12,C} & 0 \\ \sigma_{12,C} & G_C & 0 \\ 0 & 0 & G_C \end{pmatrix}, \tag{S13}$$

Through inspection of the conformation tensor, it is clear that the stress tensor and conformation tensor are directly dependent on each other, and thus, Eq. (S11) may be rewritten as:

$$\boldsymbol{\sigma_C} + \left(\frac{\eta_C(\sigma_{I,C})}{G_C}\right)\boldsymbol{\sigma_C}_{(1)} = \eta_C(\sigma_{I,C})\boldsymbol{\gamma}_{(1)} \,, \tag{S14}$$

where the governing equations for the two nonzero elements in one dimensional shear flow are:

$$\sigma_{12,C} + \left(\frac{\eta_C(\sigma_{I,C})}{G_C}\right)\frac{d\sigma_{12,C}}{dt} = \eta_C(\sigma_{I,C})\dot{\gamma} \tag{S15}$$

$$\sigma_{11,C} + \left(\frac{\eta_C(\sigma_{I,C})}{G_C}\right)\left(\frac{d\sigma_{11,C}}{dt} - 2\dot{\gamma}\sigma_{12,C}\right) = 0 \,. \tag{S16}$$

The first invariant for one dimensional shear flow is found through the summation of the diagonal components

$$\sigma_{I,C} = \mathrm{tr}(\boldsymbol{\sigma_C}) = \sigma_{11,C} + 0 + 0 = \sigma_{11,C} \,. \tag{S17}$$

To formulate the equation for the viscosity in terms of the first invariant of the stress tensor, we refer to the steady shear data where the viscosity was assumed to obey the Cross model with a unitary exponential:

$$\eta_{SS,C}(\dot{\gamma}) = \left(\frac{\mu_{0,C} - \mu_{\infty,C}}{1 + \tau_C|\dot{\gamma}|} + \mu_{\infty,C}\right). \tag{S18}$$

However, the viscosity in Eq. (S18) is directly dependent on the shear rate instead of the first invariant of the stress tensor and thus must be reformulated. Under steady shear conditions, the time derivatives in Eqs. (S15) and (S16) will be zero, and the stresses will be:

$$\sigma_{SS,12,C} = \eta_{SS,C}(\sigma_{I,C})\dot{\gamma} \,. \tag{S19}$$

$$\sigma_{SS,11,C} = 2\left(\frac{\eta_{SS,C}(\sigma_{I,C})}{G_C}\right)\dot{\gamma}\sigma_{SS,12,C} = 2\left(\frac{\eta_{SS,C}(\sigma_{I,C})^2}{G_C}\right)\dot{\gamma}^2 \,. \tag{S20}$$

Note that henceforth, the viscosity will no longer be written as a function of the first invariant of the stress tensor because it will often appear as the independent variable in the equation. From Eq. (S17), we see that Eq. (S20) equivalently gives the steady shear value for the first invariant of the stress tensor under one dimensional shear flow:

$$\sigma_{I,SS,C} = \frac{2\eta_{SS,C}^2\dot{\gamma}^2}{G_C}, \tag{S21}$$

which can be rewritten as:

$$\eta_{SS,C}\dot{\gamma} = \sqrt{\frac{G_C\sigma_{I,SS,C}}{2}}. \tag{S22}$$

From Eq. (S22), one can observe that if the viscosity is only a function of the first invariant of the stress tensor, then any definition of the viscosity in terms of other variables must feature a coupling of the shear rate with the viscosity. This differs from the original White-Metzner model which enabled the viscosity to have a direct dependence on the shear rate.

The proposed steady shear viscosity equation can be rewritten to involve a coupling of the shear rate with the viscosity by manipulating Eq. (S18):

$$\eta_{SS,C} + \left(\tau_C\left(\eta_{SS,C}\dot{\gamma}\right) - \mu_{0,C}\right) - \tau_C\mu_{\infty,C}\dot{\gamma} = 0 \tag{S23}$$

$$\eta_{SS,C}^2 + \eta_{SS,C}\left(\tau_C\left(\eta_{SS,C}\dot{\gamma}\right) - \mu_{0,C}\right) - \mu_{\infty,C}\tau_C\left(\eta_{SS,C}\dot{\gamma}\right) = 0. \tag{S24}$$

Note that the absolute value in Eq. (S18) has been dropped because all flows considered in this work are in the positive direction. However, the model can still handle flow reversals but will require a conditional expression. Eq. (S24) is a quadratic equation which can be solved for the viscosity as a function of the first invariant of the stress tensor by utilizing the relation in Eq. (S22):

$$a = 1 \tag{S25}$$

$$b = \tau_C\sqrt{\frac{G_C\sigma_{I,C}}{2}} - \mu_{0,C} \tag{S26}$$

$$c = -\mu_{\infty,C}\tau_C\sqrt{\frac{G_C\sigma_{I,C}}{2}} \tag{S27}$$

$$\eta_C\left(\sigma_{I,C}\right) = \frac{-b-\sqrt{b^2-4ac}}{2a}. \tag{S28}$$

In Eqs. (S25-S28), the subscripts denoting steady shear have been dropped as the viscosity will have the same dependence on the first invariant of the stress tensor for any transient flow. This proposed form for the viscosity will reduce to Eq. (S18) under steady conditions.

It should be noted that the same steady shear behavior for the viscosity could also be obtained by eliminating the infinite shear viscosity from the extended White-Metzner model then adding it back to the total stress as is common with equations of motion for polymers. However, this approach is not suitable for this system as the red blood cells are deforming against the bulk even at high shear rates. Additionally, if this approach were used, the elastic effects would disappear at high shear rates. This disappearance is not observed in the experimental data.

S-III. MODEL FITTING PARAMETERS

The 10 successive runs and corresponding optimal values for the high shear, steady state model parameters are shown in Tables S-I and S-II for Donor 1 and 2 respectively. Note that the high shear parameters were determined through a fit of the model with the structure components set to zero to the steady shear data at shear rates greater than 20 s^{-1}. The variations between the 10 runs are very small, indicating the high certainty in the evaluation of the optimal parameters for the data set.

TABLE S-I. Optimal high shear, steady state model parameters for data from Donor 1 for each of the 10 parallel runs. The 10 runs are shown for the steady shear data obtained at both the beginning and end of the experiments. The runs with the lowest objective value are bolded in blue.

Run	Beginning				End			
	$\mu_{0,C}$ (mPa.s)	$\mu_{\infty,C}$ (mPa.s)	τ_C (s)	F_{obj}	$\mu_{0,C}$ (mPa.s)	$\mu_{\infty,C}$ (mPa.s)	τ_C (s)	F_{obj}
1	7.8227	3.0724	0.038288	1.4257E-5	7.4370	3.2309	0.031595	7.1666E-5
2	7.8216	3.0724	0.038278	1.4256E-5	7.4379	3.2309	0.031602	7.1666E-5
3	7.8253	3.0724	0.038321	1.4256E-5	7.4376	3.2310	0.031603	7.1666E-5
4	7.8226	3.0724	0.038286	1.4256E-5	7.4373	3.2310	0.031601	7.1666E-5
5	7.8204	3.0723	0.038262	1.4257E-5	**7.4378**	**3.2310**	**0.031603**	**7.1666E-5**
6	7.8187	3.0723	0.038240	1.4257E-5	7.4383	3.2310	0.031608	7.1666E-5
7	**7.8242**	**3.0724**	**0.038302**	**1.4256E-5**	7.4431	3.2311	0.031664	7.1668E-5
8	7.8250	3.0724	0.038309	1.4256E-5	7.4370	3.2309	0.031594	7.1666E-5
9	7.8205	3.0724	0.038268	1.4257E-5	7.4379	3.2310	0.031607	7.1666E-5
10	7.8237	3.0724	0.038301	1.4256E-5	7.4372	3.2309	0.031597	7.1666E-5

TABLE S-II. Optimal high shear, steady state model parameters for data from Donor 2 for each of the 10 parallel runs. The 10 runs are shown for the steady shear data obtained at both the beginning and end of the experiments. The runs with the lowest objective value are bolded in red.

Run	Beginning				End			
	$\mu_{0,C}$ (mPa.s)	$\mu_{\infty,C}$ (mPa.s)	τ_C (s)	F_{obj}	$\mu_{0,C}$ (mPa.s)	$\mu_{\infty,C}$ (mPa.s)	τ_C (s)	F_{obj}
1	**8.5589**	**3.4984**	**0.036117**	**1.6211E-5**	10.275	4.0221	0.037546	3.7301E-5
2	8.5564	3.4984	0.036099	1.6211E-5	10.275	4.022	0.037534	3.7300E-5
3	8.5552	3.4984	0.036086	1.6212E-5	10.275	4.0221	0.037538	3.7300E-5
4	8.5600	3.4984	0.036128	1.6211E-5	10.282	4.0222	0.037600	3.7300E-5
5	8.5589	3.4984	0.036119	1.6211E-5	10.324	4.0228	0.037944	3.7395E-5
6	8.5287	3.4979	0.035822	1.6263E-5	10.278	4.0221	0.037558	3.7299E-5
7	8.5684	3.4985	0.036214	1.6216E-5	**10.279**	**4.0221**	**0.037573**	**3.7299E-5**
8	8.5609	3.4984	0.036141	1.6211E-5	10.281	4.0221	0.037587	3.7299E-5
9	8.5951	3.4990	0.036491	1.6284E-5	10.281	4.0222	0.037584	3.7300E-5
10	8.5580	3.4983	0.036106	1.6211E-5	10.290	4.0223	0.037663	3.7306E-5

The 10 successive runs and corresponding optimal values for the low shear, steady state model parameters are shown in Tables S-III and S-IV for Donor 1 and 2 respectively. Note that the low shear parameters were determined through a fit of the full model to the full steady shear data. The high shear parameters were fixed for each flow curve as the previously determined optimal parameter set. The

variations between the 10 runs are very small, indicating the high certainty in the evaluation of the optimal parameters for the data set.

TABLE S-III. Optimal low shear, steady state model parameters for data from Donor 1 for each of the 10 parallel runs. The 10 runs are shown for the steady shear data obtained at both the beginning and end of the experiments. The runs with the lowest objective value are bolded in blue.

	Beginning				End			
Run	σ_y (mPa)	τ_a (s)	μ_R (mPa.s)	F_{obj}	σ_y (mPa)	τ_a (s)	μ_R (mPa.s)	F_{obj}
1	1.6123	482.74	9.2235	1.6354E-5	2.3028	561.28	9.9429	7.1629E-5
2	1.6126	482.70	9.2236	1.6354E-5	2.3026	561.29	9.9429	7.1629E-5
3	1.6128	482.74	9.2225	1.6354E-5	2.3027	561.30	9.9428	7.1629E-5
4	1.6126	482.72	9.2233	1.6354E-5	2.3026	561.31	9.9429	7.1629E-5
5	1.6121	482.69	9.2245	1.6354E-5	2.3029	561.30	9.9426	7.1629E-5
6	1.6125	482.74	9.2227	1.6354E-5	**2.3027**	**561.30**	**9.9429**	**7.1629E-5**
7	**1.6126**	**482.73**	**9.2232**	**1.6354E-5**	2.3023	561.27	9.944	7.1629E-5
8	1.6126	482.75	9.2227	1.6354E-5	2.3025	561.29	9.9434	7.1629E-5
9	1.6125	482.72	9.2237	1.6354E-5	2.3025	561.31	9.9428	7.1629E-5
10	1.6126	482.72	9.2233	1.6354E-5	2.3025	561.27	9.9439	7.1629E-5

TABLE S-IV. Optimal low shear, steady state model parameters for data from Donor 2 for each of the 10 parallel runs. The 10 runs are shown for the steady shear data obtained at both the beginning and end of the experiments. The runs with the lowest objective value are bolded in red.

Run	Beginning				End			
	σ_y (mPa)	τ_a (s)	μ_R (mPa.s)	F_{obj}	σ_y (mPa)	τ_a (s)	μ_R (mPa.s)	F_{obj}
1	1.2284	384.93	30.936	3.3557E-5	**3.1667**	**410.75**	**40.999**	**6.0209E-5**
2	1.2285	384.94	30.935	3.3557E-5	3.1663	410.74	41.001	6.0209E-5
3	1.2286	384.93	30.935	3.3557E-5	3.1676	410.74	40.999	6.0209E-5
4	1.2287	384.94	30.935	3.3557E-5	3.1668	410.73	41.000	6.0209E-5
5	1.2291	384.95	30.933	3.3557E-5	3.1665	410.73	41.000	6.0209E-5
6	1.2281	384.94	30.936	3.3557E-5	3.1675	410.75	40.998	6.0209E-5
7	1.2291	384.95	30.933	3.3557E-5	3.1663	410.73	41.003	6.0209E-5
8	1.2283	384.93	30.936	3.3557E-5	3.1669	410.72	41.002	6.0209E-5
9	**1.2287**	**384.94**	**30.935**	**3.3557E-5**	3.1672	410.75	40.999	6.0209E-5
10	1.2289	384.94	30.934	3.3557E-5	3.1666	410.74	41.001	6.0209E-5

The 10 successive runs and corresponding optimal values for the transient model parameters are shown in Tables S-V and S-VI for Donor 1 and 2 respectively. Note that the transient parameters were determined through a simultaneous fit of the model to four UD-LAOS curves described in the main text. The steady state parameters, with the exception of τ_a, for each UD-LAOS curve were specified as the stress weighted average of the beginning and ending values for the steady state flow curves. The UD-LAOS preshear and the corresponding stress at the steady shear flow curves were used as the weighting factor and bounds respectively. The error associated with the parameter estimation was taken as the standard deviation of the 10 successive runs.

TABLE S-V. Optimal transient model parameters for data from Donor 1 for each of the 10 parallel runs. The run with the lowest objective value is bolded in blue.

Run	G_C (Pa)	τ_λ (s)	τ_G (s)	F_{obj}
1	0.44778	1958.9	1.6566	0.0027636
2	0.43017	1907.8	1.5722	0.0027648
3	0.42618	1927.0	1.6179	0.0027652
4	0.42857	1927.9	1.5821	0.0027660
5	**0.44799**	**1960.2**	**1.6580**	**0.0027636**
6	0.43871	1941.4	1.5842	0.0027655
7	0.42630	1909.9	1.5826	0.0027650
8	0.42814	1915.0	1.6451	0.0027646
9	0.43476	1920.5	1.6113	0.0027649
10	0.42831	1906.1	1.5840	0.0027647

TABLE S-VI. Optimal transient model parameters for data from Donor 2 for each of the 10 parallel runs. The run with the lowest objective value is bolded in red.

Run	G_C (Pa)	τ_λ (s)	τ_G (s)	F_{obj}
1	0.64594	1574.3	1.6443	0.0018554
2	0.61965	1568.4	1.6457	0.0018547
3	0.62600	1576.1	1.6971	0.0018546
4	0.61664	1575.1	1.6612	0.0018550
5	**0.63899**	**1597.1**	**1.7090**	**0.0018546**
6	0.61755	1537.6	1.6444	0.0018550
7	0.62781	1561.0	1.7789	0.0018567
8	0.62937	1547.9	1.5524	0.0018570
9	0.63307	1534.2	1.6042	0.0018551
10	0.66626	1568.7	1.7568	0.0018580

S-IV. ADDITIONAL FIGURES

The steady state structure parameter value as a function of shear rate is shown for both donors in Fig. S1. As expected, both donors show a similar trend with the structure parameter at approximately 1 at low shear rates and declining to 0 at high shear rates. The structure parameter for Donor 1 is higher than that of Donor 2 at a particular shear rate. This observable difference is likely linked to the difference in physiology between the two samples.

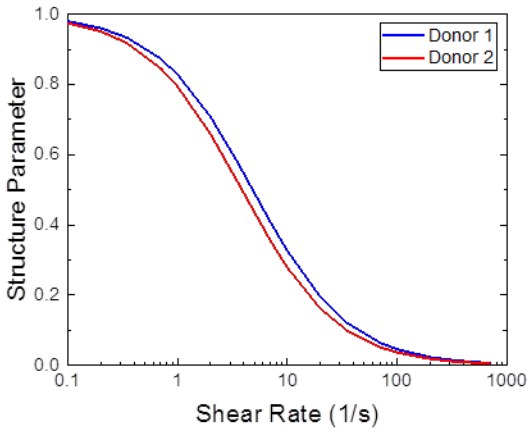

FIG. S1. Structure parameter as a function of the shear rate for the initial steady shear flow curves for both donors.

The viscous projections for experimental data for the four UD-LAOS curves used for fitting and corresponding model fits for Donor 1 and Donor 2 are shown in Figs. S2 and S3 respectively. Inspection of the viscous projections shows a primarily viscous behavior with seemingly no elastic effects present at the low frequency shown in Figs. S2(c) and S3(c).

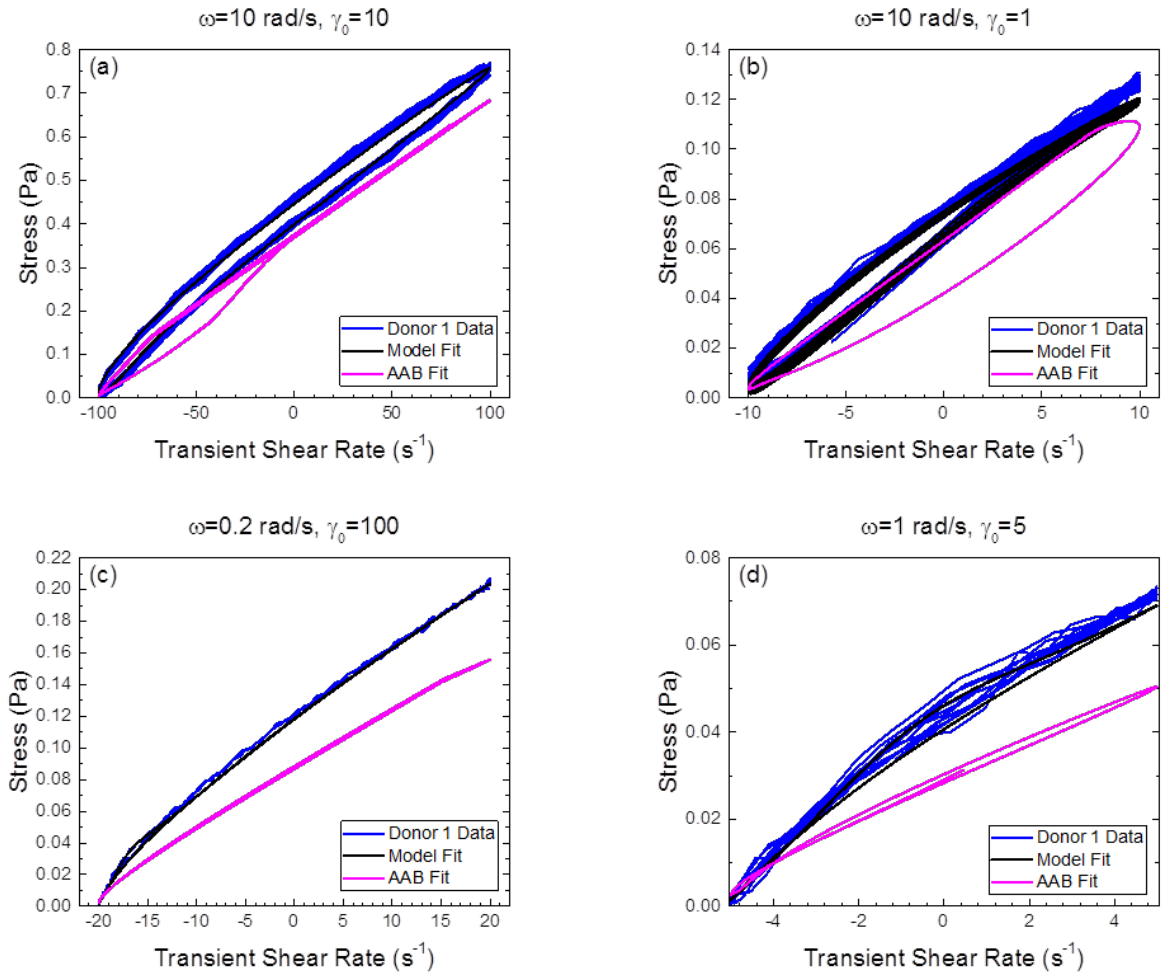

FIG. S2. Viscous projection model fit to UD-LAOS experimental data on blood from Donor 1 at (a) a frequency of 10 rad/s and a strain amplitude of 10, (b) a frequency of 10 rad/s and a strain amplitude of 1, (c) a frequency of 0.2 rad/s and a strain amplitude of 100, and (d) a frequency of 1 rad/s and a strain amplitude of 5.

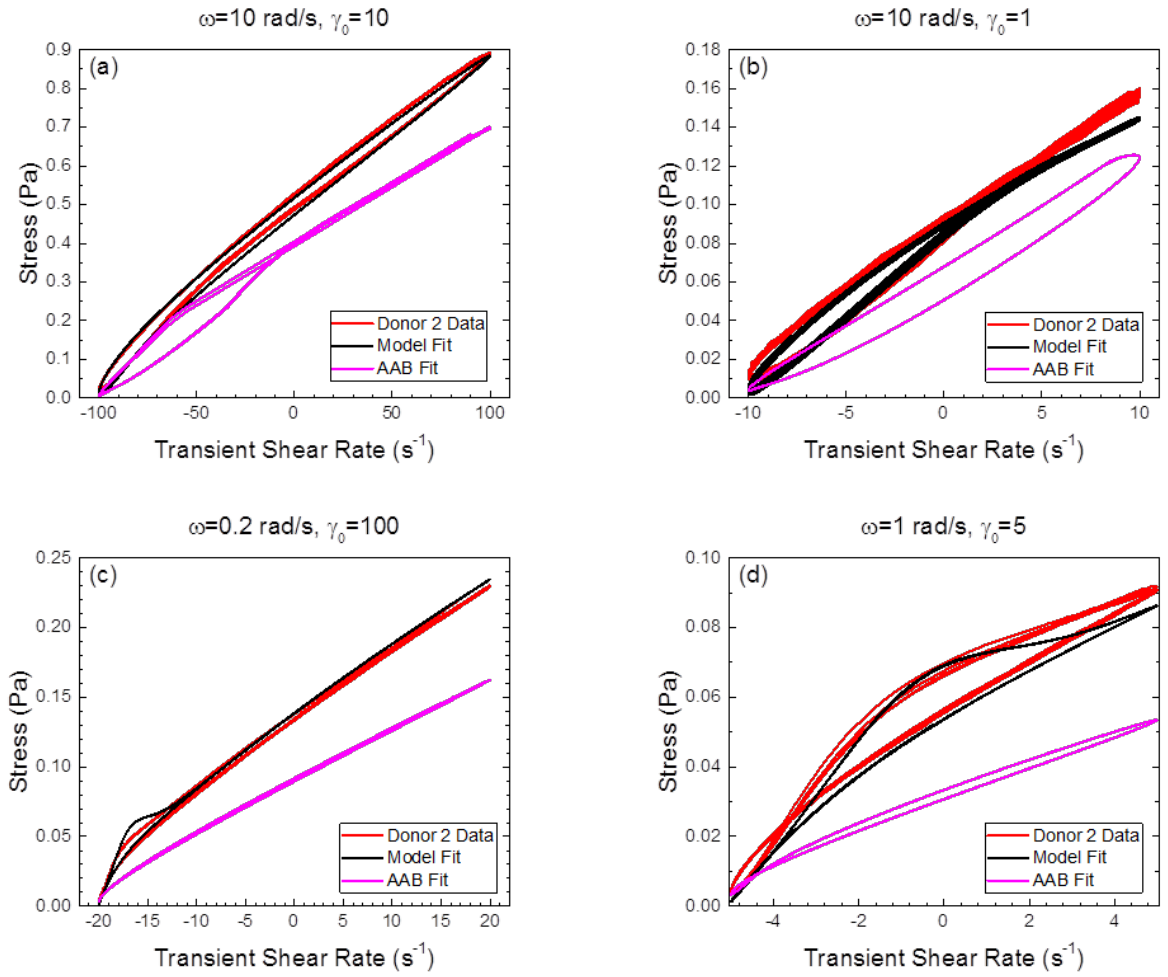

FIG. S3. Viscous projection model fit to UD-LAOS experimental data on blood from Donor 2 at (a) a frequency of 10 rad/s and a strain amplitude of 10, (b) a frequency of 10 rad/s and a strain amplitude of 1, (c) a frequency of 0.2 rad/s and a strain amplitude of 100, and (d) a frequency of 1 rad/s and a strain amplitude of 5.

The elastic projections for the structure parameter during the four UD-LAOS curves used for fitting for Donor 1 and Donor 2 are shown in Fig. S4. The viscous projections are shown in Fig. S5. Inspection of the structure parameter value enables insight into the different transient structure processes between the two blood samples. Note that the structure parameter is consistently higher for blood from Donor 1.

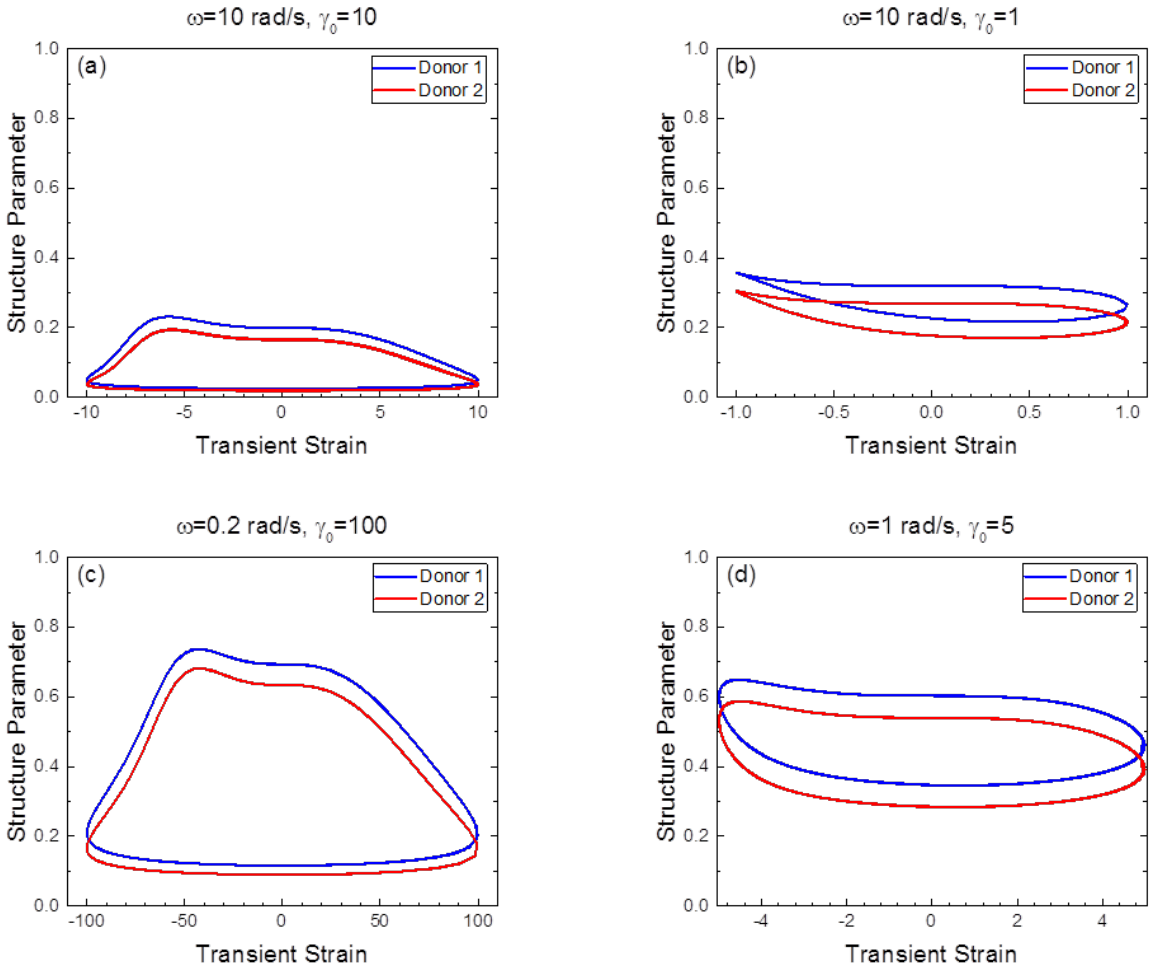

FIG. S4. Elastic projection structure parameter value for UD-LAOS experiments on blood from both donors at (a) a frequency of 10 rad/s and a strain amplitude of 10, (b) a frequency of 10 rad/s and a strain amplitude of 1, (c) a frequency of 0.2 rad/s and a strain amplitude of 100, and (d) a frequency of 1 rad/s and a strain amplitude of 5.

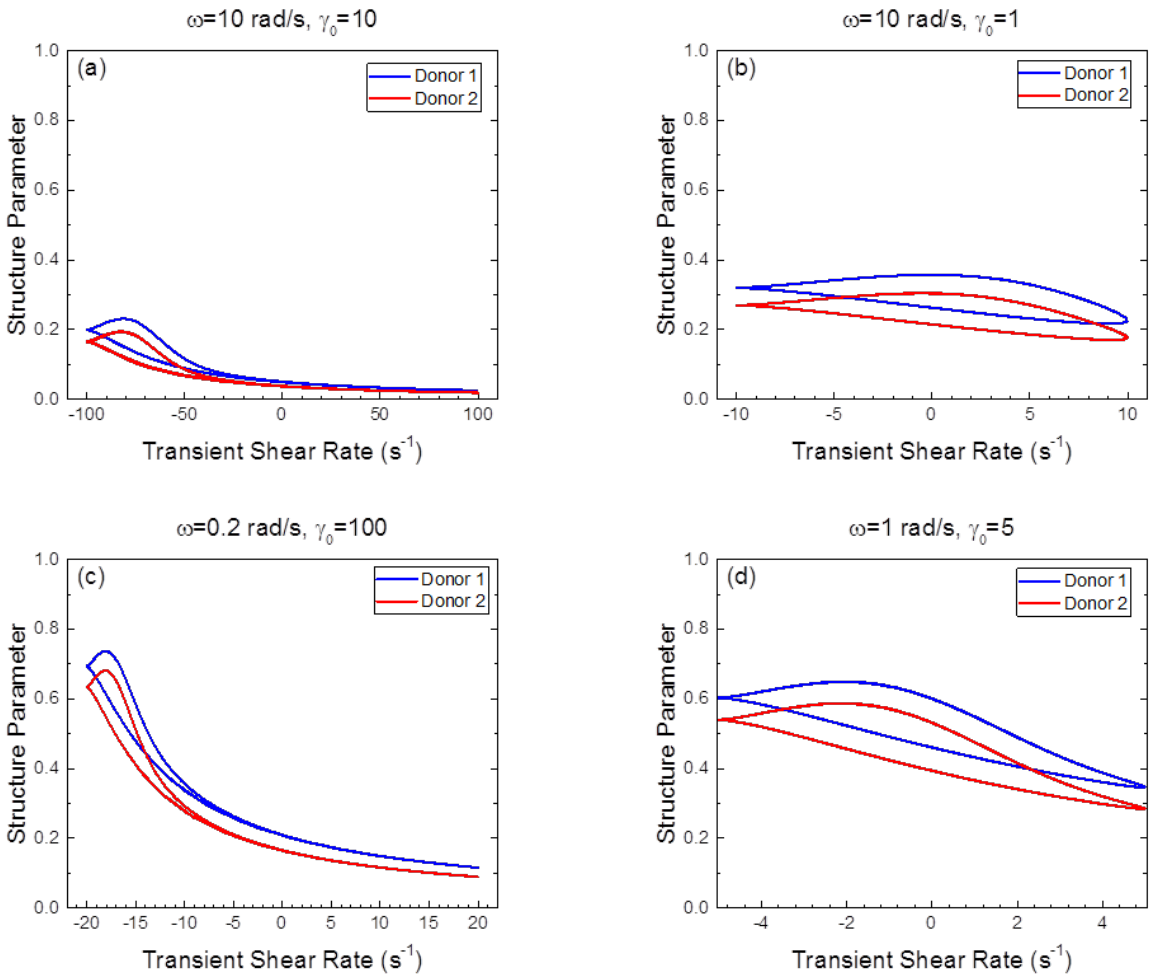

FIG. S5. Viscous projection structure parameter value for UD-LAOS experiments on blood from both donors at (a) a frequency of 10 rad/s and a strain amplitude of 10, (b) a frequency of 10 rad/s and a strain amplitude of 1, (c) a frequency of 0.2 rad/s and a strain amplitude of 100, and (d) a frequency of 1 rad/s and a strain amplitude of 5.

The Pipkin diagram of the viscous UD-LAOS projections for Donor 2 and corresponding model fits is shown in Fig. S6. Inspection shows that over most frequencies and amplitudes the elastic effects are small. However, small elastic effects exist at low strain amplitudes as well as at high frequencies and high strain amplitudes. Additionally, thixotropic effects may be observed at moderate to low strain amplitudes and moderate frequencies.

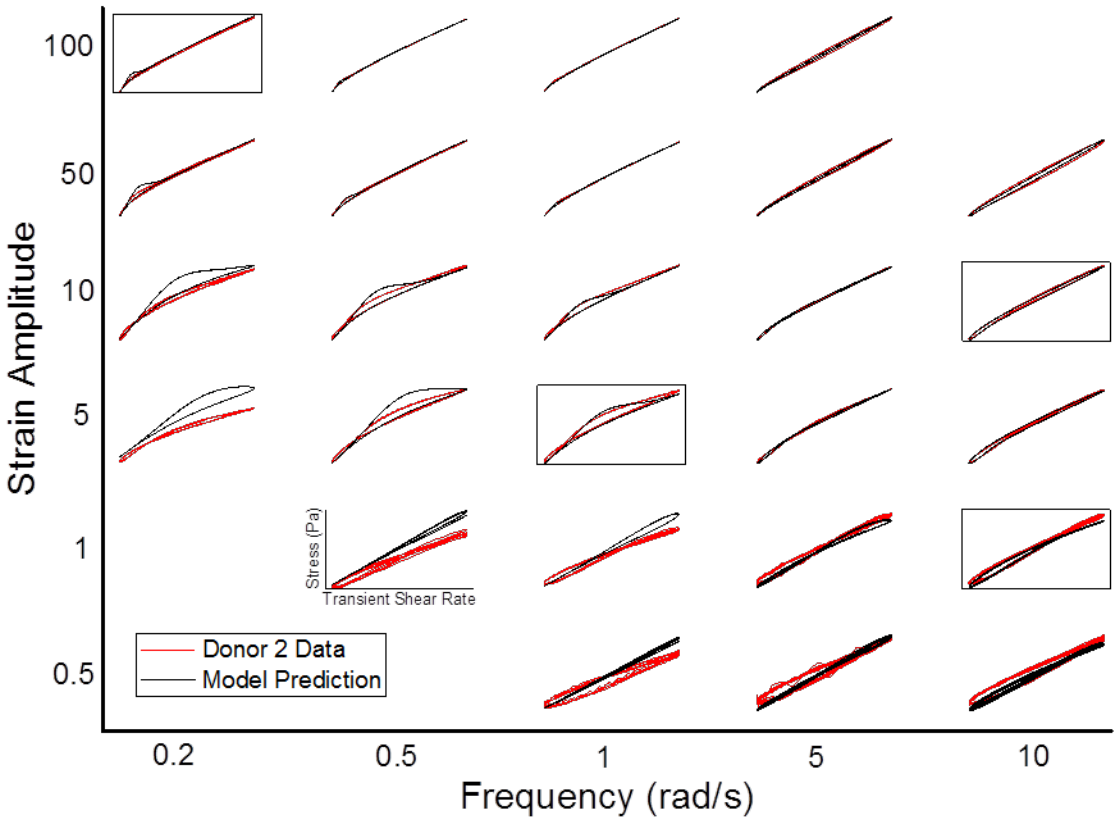

FIG. S6. Pipkin diagram of UD-LAOS viscous projections for blood from Donor 2. The model predictions are also shown with the four curves used to fit the parameters boxed.